

## Hydrogenation of naphthalene and anthracene on Pt/C catalysts

A. N. Kalenchuk,<sup>a,b</sup> A. E. Koklin,<sup>b</sup> V. I. Bogdan,<sup>a,b</sup> and L. M. Kustov<sup>a,b</sup>

<sup>a</sup>Department of Chemistry, M. V. Lomonosov Moscow State University,  
1/3 Leninskie Gory, 119991 Moscow, Russian Federation

<sup>b</sup>N. D. Zelinsky Institute of Organic Chemistry, Russian Academy of Sciences,  
47 Leninsky prop., 119991 Moscow, Russian Federation.  
Fax: +7 (499) 137 2935. E-mail: akalenchuk@yandex.ru

Hydrogenation of naphthalene and anthracene deposited on Sibunit and active carbon was studied. The reactions were carried out at a temperature of 280 °C and a pressure of 90 atm. The directions for the complete hydrogenation of the investigated substrates were studied. Correlations between the structures of naphthalene and anthracene and their activity in hydrogen absorption are presented. The hydrogenation rates decrease as the substrate is saturated with hydrogen.

**Key words:** hydrogenation, naphthalene, anthracene, decalin, perhydroanthracene, Pt/C.

Last years, power engineering of hydrogen fuel cells (HFCs) has been actively developed world wide. Among factors that restrain wide use of HFCs is the absence of compact and safe systems of storage with a high hydrogen capacity, which are capable of ensuring a completed rapid charging and hydrogen evolution. It is known that in chemical compounds hydrogen atoms are packed as close as possible.<sup>1</sup> Among them aromatic hydrocarbons play a special role, since they have the hydrogen capacity higher than 7 wt.% and can multiply absorb and evolve chemically pure hydrogen without impurities of  $\text{CO}_x$  gases in the course of reversible catalytic reactions of hydrogenation—dehydrogenation.<sup>2,3</sup> The monocyclic systems, such as benzene/cyclohexane and toluene/methylcyclohexane, dehydrogenation and hydrogenation processes of which are widely used in industry, are the most studied hydrogen storage materials.<sup>4–8</sup> However, many problems directly concerning processes of hydrogen accumulation and generation remain still unclear. This is especially true for cyclic compounds with many rings.<sup>9,10</sup> For example, different mechanisms of adsorption can be involved in the hydrogenation of aromatic molecules on the Pt catalysts, while accessibility of some C—C bonds decreases with increasing degree of condensation.<sup>11–14</sup> In particular, the hydrogenation rates for a series of linearly conjugated biphenyl and terphenyl molecules observed on Pt/C catalysts were lower than that for benzene.<sup>2,15</sup> Stereoisomers of terphenyl also showed different characters of hydrogenation,<sup>15</sup> which also affects the hydrogen charging for storage systems based on these hydrocarbons.

In this work, we compared the liquid-phase hydrogenation of naphthalene and anthracene with that of benzene on the Pt/C catalysts. The purpose of the investigation is

to reveal and study the features of hydrogenation of polycyclic hydrocarbons with different degrees of condensation.

### Experimental

**Catalysts.** The catalyst 3%Pt/Sibunit on the carbon support Sibunit (Institute of Problems of Hydrocarbons Processing, Siberian Branch, Russian Academy of Sciences, Omsk;  $\rho = 0.62 \text{ g cm}^{-3}$ ) with the granule size  $d = 1.5\text{--}1.8 \text{ mm}$  was used for hydrogenation. Platinum was deposited on the surface by the impregnation of the support with an aqueous solution of  $[\text{H}_2\text{PtCl}_6]$  using the incipient wetness impregnation method according to a known procedure.<sup>2</sup> The catalyst 3%Pt/C (Aldrich, lot No. 06523VT;  $\rho = 0.32 \text{ g cm}^{-3}$ ) on active carbon ( $d < 0.1 \text{ mm}$ ) was used for comparison. Prior to reactions, the catalysts were activated for 2 h in a hydrogen flow ( $30 \text{ mL min}^{-1}$ ) at 305 °C. The specific surface area ( $S_{\text{BET}}$ ) of the catalysts was determined by the method of low-temperature nitrogen sorption using the polymolecular BET model. The particle size ( $R$ ) and dispersity of Pt ( $D$ ) were determined on an ASAP 2020 microanalyzer (USA) using the method of irreversible chemisorption of CO at 35 °C. The morphology of the catalyst surface was studied by scanning electron microscopy (SEM) with field emission on a Hitachi SU8000 electron microscope. Images were recorded in the secondary electron detection mode at an accelerating voltage of 2–30 kV and a working distance of 8–10 mm. The microstructure of the samples was studied by transmission electron microscopy (TEM) on a Hitachi HT7700 electron microscope. Images were recorded in the light field mode at an accelerating voltage of 100 kV.

**Substrates.** The following chemical reagents without impurities of sulfur compounds and other chemical poisons of catalysts were used as substrates: benzene (Acros Organics, 99.5%; m.p. 5–6 °C, b.p. 80 °C,  $\rho = 0.88 \text{ g cm}^{-3}$ ), naphthalene (Acros Organics, 99%; m.p. 80–82 °C, b.p. 217 °C,  $\rho = 1.14 \text{ g cm}^{-3}$ ),

and anthracene (Aldrich, 97%; m.p. 218 °C, b.p. 340 °C,  $\rho = 1.25 \text{ g cm}^{-3}$ ).

**Kinetic experiment.** One volume of the catalyst and 10 volumes of substrate ( $10 \text{ cm}^3 : 100 \text{ cm}^3$ ) were charged in a PARR-5500 high-pressure autoclave (USA) with a volume of 600 mL. The liquid-phase hydrogenation of naphthalene and anthracene with mechanical stirring (600 rpm) was conducted at 280 °C and 90 atm, and benzene was hydrogenated at 180 °C and 70 atm.

At certain intervals, the reaction was stopped and the samples were taken for the analysis. The composition of the reaction products was analyzed on a KristalLyks-4000M chromatograph (Khromatek, Russia) with the ZB-5 (Zebron, USA) and TR-FFAP (Thermo Scientific, USA) capillary columns with a flame-ionization detector and on a FOCUS DSQ II mass spectrometer coupled with chromatograph (MS/GC) (Thermo Fisher Scientific, USA) with the TR-5MS capillary column (Thermo, USA). The conversion ( $X$ ) and selectivity ( $S$ ) of the hydrogenation products were calculated by the equations

$$X = [(c_0 - c)/c_0] \cdot 100\%,$$

$$S = [\Sigma c(i)/\Sigma c(k)] \cdot 100\%,$$

where  $c_0$  and  $c$  are the initial and final concentrations of the starting substrate, respectively; and  $\Sigma c(i)$  and  $\Sigma c(k)$  are the sums of concentrations of individual products and all reaction products, respectively.

## Results and Discussion

According to the SEM data, the catalyst surface on the active carbon 3%Pt/C (Aldrich) consists of aggregates formed by particles of varying shape larger than 2 μm in size.<sup>16</sup> The 3%Pt/Sibunit catalyst has a more ordered surface formed of numerous particles less than 1 μm. The uniform distribution of Pt is observed on the TEM images of both studied catalysts. The histograms of the particle size distribution of both catalysts were calculated from their TEM images. It is seen that fine clusters (to 2 nm) mainly located on the external surface of the Sibunit globules prevail in the Sibunit-based catalysts. The catalyst on active carbon has a broader particle size distribution ( $d_{av} = 7 \text{ nm}$ ). The porous structure of active carbons is characterized by the presence of all types of pores with the following pore sizes and specific volumes: submicro- and micropores (to 2 nm,  $0.2\text{--}0.6 \text{ cm}^3 \text{ g}^{-1}$ ), mesopores ( $2\text{--}50 \text{ nm}$ ,  $0.15\text{--}0.2 \text{ cm}^3 \text{ g}^{-1}$ ), and macropores ( $>50 \text{ nm}$ ,  $0.02\text{--}0.10 \text{ cm}^3 \text{ g}^{-1}$ ).<sup>17</sup> Sibunit is a predominantly mesoporous material. According to the data of CO chemisorption, the average pore size in Sibunit used as a support in the catalyst studied is 6 nm.<sup>18</sup>

The texture characteristics of the catalysts 3%Pt/Sibunit and 3%Pt/C (Aldrich) are presented in Table 1. A comparison with the data in Fig. 1 shows that the sizes of platinum clusters determined by the chemisorption method and electron microscopy are comparable. The catalyst on Sibunit has a higher dispersity, smaller sizes

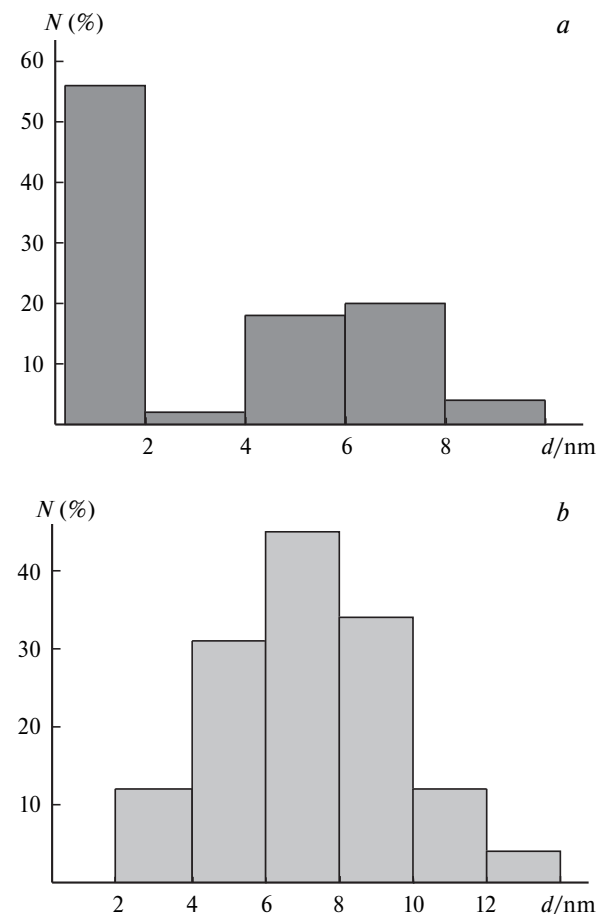


Fig. 1. Histograms of the Pt particle size distribution for the catalysts 3%Pt/Sibunit (a) and 3%Pt/C (Aldrich) (b).

of the platinum clusters, and a substantially lower specific surface area. However, the times of complete benzene hydrogenation for both catalysts do not differ within the experimental error. The 95% conversion of benzene on the both catalysts is achieved approximately 20 min after the reaction onset, whereas the complete hydrogenation is attained in 24 min. Similar catalytic activities of both samples can be related to blocking of some Pt atoms in the active carbon-based catalyst micropores, which decreases the fraction of the accessible surface of active metal.<sup>19</sup>

Table 1. Texture characteristics of the Pt/C catalysts

Catalyst	Bulk density /g cm <sup>-3</sup>	$S_{BET}^a$ /m <sup>2</sup> g <sup>-1</sup>	$D^b$ (%)	$R^c$ /nm
3%Pt/Sibunit	0.65	300	49	2.5
3%Pt/C (Aldrich)	0.32	760	22	5.5

<sup>a</sup> Surface area.

<sup>b</sup> Dispersity of Pt.

<sup>c</sup> Particle size of Pt.

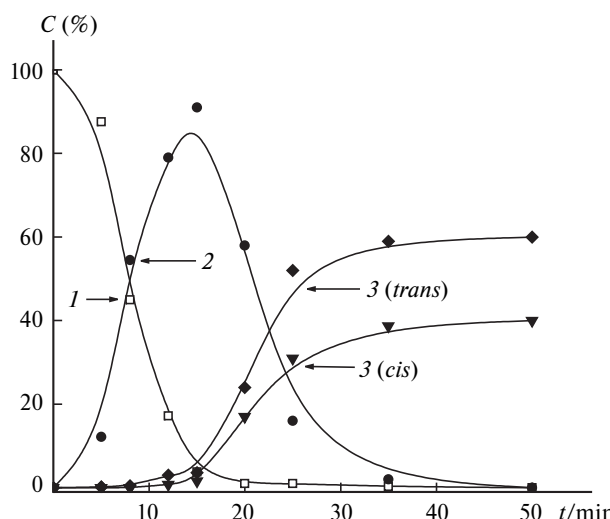
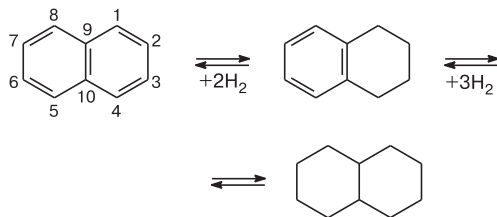


**Fig. 2.** Concentration of the products of naphthalene hydrogenation as a function of the reaction time: 1,  $C_{10}H_8$ ; 2,  $C_{10}H_{12}$ ; and 3,  $C_{10}H_{18}$ .

The experimental time dependences of the concentration of the hydrogenation products of naphthalene ( $C_{10}H_8$ ) on the 3%Pt/C catalyst (Aldrich) are shown in Fig. 2. Curve 3 in Fig. 2 describes the kinetics of tetralin formation and has a characteristic "induction period" indicating that decalin (decahydronaphthalene,  $C_{10}H_{18}$ ) is not formed directly but *via* the intermediate product tetralin (1,2,3,4-tetrahydronaphthalene,  $C_{10}H_{12}$ ). The concentration of tetralin increases from zero, passes through a maximum, and again decreases to zero (see Fig. 2, curve 2). The dependence of the naphthalene consumption on time (see Fig. 2, curve 1) is described by an S-like curve, according to which the concentration decreases rapidly to the moment of formation of a maximum on the curve of tetralin and then decreases slowly to zero. The hydrogenation of naphthalene can be presented as general Scheme 1.

**Scheme 1**



In a naphthalene molecule, four C(1)—C(2) bonds are shorter than those in benzene (1.365 Å) and two C(2)—C(3) bonds (1.404 Å), four C(4)—C(10) bonds (1.420 Å), and the distance between the C(9)—C(10) nodal atoms (1.420 Å) are longer, which leads to a distortion of symmetry of two fused benzene rings.<sup>13,20</sup> The symmetry of the benzene

ring in tetralin improves,<sup>21</sup> but the cyclohexane "chair" violates coplanarity of the molecule to induce steric hindrances for the interaction with the catalyst. It is seen from Fig. 2 that the maximum on the curve of tetralin formation is achieved within 15 min, and the curve of decalin formation reaches a plateau already within 35 min. Fifty minutes are required for the complete saturation of naphthalene on the catalyst at 99.5% conversion. Figure 2 also shows that about 15 min are needed to achieve 95% conversion for naphthalene hydrogenation, less time than required to convert 95% of benzene. The final hydrogenation product, decalin, consists of a mixture of *trans*- (60 wt.%) and *cis*-isomer (40 wt.%). The overall selectivity of two isomers exceeds 99.5%. For the complete saturation of naphthalene with hydrogen on the 3%Pt/Sibunit catalyst ~60 min are needed, and the shape of the curves and the ratio of formed isomers remain unchanged.

The experimental curves showing a change in the concentrations of the hydrogenation products of anthracene ( $C_{14}H_{10}$ ) on the 3%Pt/C (Aldrich) catalyst in time are presented in Fig. 3. Perhydroanthracene ( $C_{14}H_{24}$ ) is the product of the complete hydrogenation of anthracene. The induction period on curve 5 (see Fig. 3) also indicates the formation of perhydroanthracene *via* intermediates. The chromatographic and MS/GC analyses showed that 9,10-dihydroanthracene ( $C_{14}H_{12}$ ), 1,2,3,4-tetrahydroanthracene ( $C_{14}H_{14}$ ), and isomers of octahydroanthracene ( $C_{14}H_{18}$ ) with different arrangements of the last unsaturated ring are formed as intermediate products of the reaction. No compounds with incompletely saturated benzene rings, such as hexahydroanthracene ( $C_{14}H_{16}$ ), decahydroanthracene ( $C_{14}H_{20}$ ), and dodecahydroanthracene ( $C_{14}H_{22}$ ), were found among the reaction products. According to the stoichiometry of formation of the observed reaction products, the hydrogenation of anthracene can be presented as general Scheme 2.

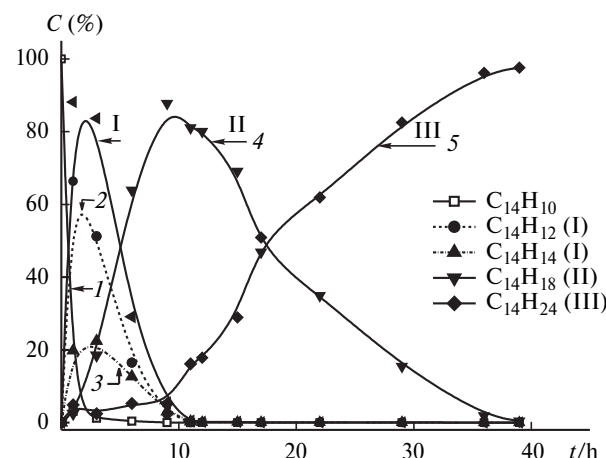
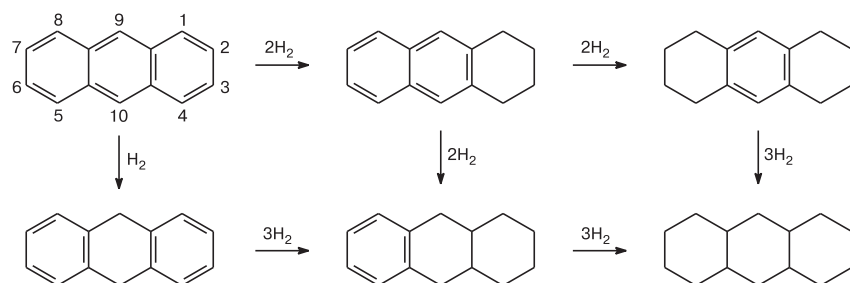


**Fig. 3.** Concentration of the products of anthracene hydrogenation as a function of the reaction time (see clarifications in the text).

Scheme 2



In Fig. 3, all compounds obtained are graphically combined into three groups according to the degree of saturation of aromatic rings. Group I of compounds with one cyclohexane ring contains 9,10-dihydroanthracene and 1,2,3,4-tetrahydronanthracene. Octahydroanthracene isomers form group III of compounds with two saturated rings. Group III includes conformers of perhydroanthracene. The total concentrations taking into account all found isomeric compounds for groups II and III are shown in Fig. 3 (curves 4 and 5, respectively).

The symmetry of benzene rings in an anthracene molecule is also violated compared to the symmetry of a benzene molecule. The central ring with four C(9)—C(11) distances of 1.400 Å is distorted to a lesser extent than both terminal rings with four C(1)—C(2) distances of 1.370 Å, two C(2)—C(3) distances of 1.410 Å, and four C(1)—C(11) distances of 1.463 Å. Both bonds between the nodal atoms lengthen compared to those in naphthalene and are equal to 1.450 Å each.<sup>13,20</sup> The curve of changing the anthracene concentration in time on the 3%Pt/C catalyst (Aldrich) (see Fig. 3, curve 1) resemble in shape the curve for naphthalene. However, about 60 min are required to achieve 95% conversion of anthracene, which exceeds the time found for naphthalene. The same conversion of anthracene on the 3%Pt/Sibunit catalyst is achieved approximately 10 min later.

The presence of two terminal benzene rings on the central ring favors an increase in the reactivity of anthracene in positions C(9) and C(10) Å.<sup>13,20</sup> It is seen from Fig. 3 that the amount of 9,10-dihydroanthracene found in analysis of the samples (see Fig. 3, curve 2) exceeds the amount of 1,2,3,4-tetrahydronanthracene (see Fig. 3, curve 3) approximately threefold. A 9,10-dihydroanthracene molecule can structurally be characterized as tetralin shielded by the benzene ring, and 1,2,3,4-tetrahydronanthracene can be presented as naphthalene shielded by the cyclohexane ring. According to this representation and results of naphthalene hydrogenation, a lower concentration of 1,2,3,4-tetrahydronanthracene in the products (see Fig. 3, curve 3) is possibly attributed to a higher rate of its conversion to octahydroanthracene compared to 9,10-dihydroanthracene. It is seen that additional violations of coplanarity

of molecules of both compounds favor the enhancement of steric hindrances for the interaction with the catalyst. The conversion for both intermediates as high as 95% is achieved in approximately 10 h after the reaction onset under the experimental conditions used.

The major product of a deeper hydrogenation of 9,10-dihydroanthracene and 1,2,3,4-tetrahydronanthracene is 1,2,3,4,5,6,7,8-octahydroanthracene (Fig. 4, a, curve 3) with the central (sym-) benzene ring and two stereoisomers of octahydroanthracene with the terminal benzene ring:

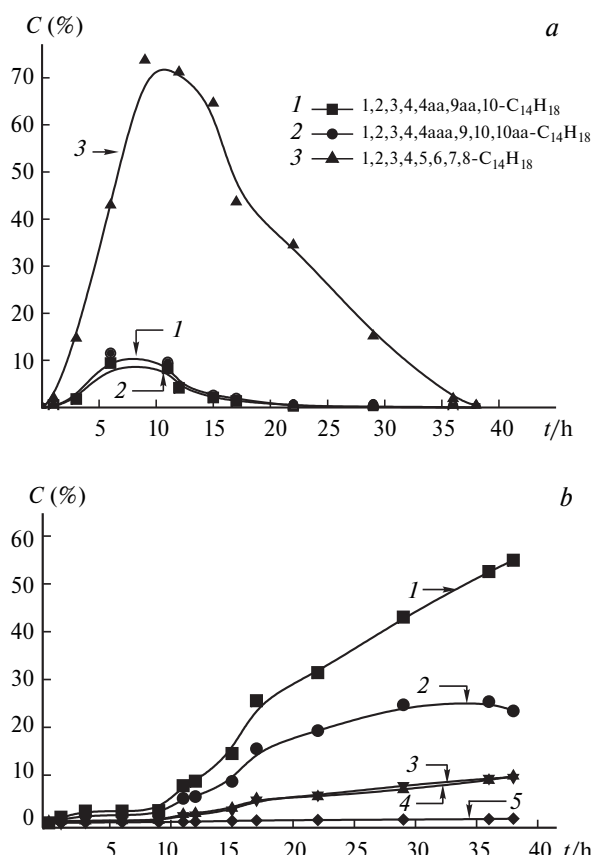


**Fig. 4.** Concentration of isomers of octahydroanthracene (1–3) (a) and perhydroanthracene (1–5) (b) formed during anthracene hydrogenation as a function of the reaction time.

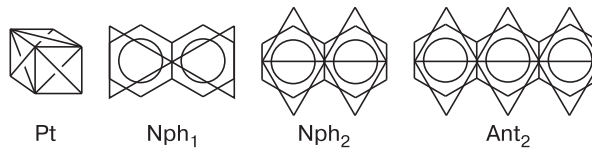
1,2,3,4,4aa,9,9aa,10- and 1,2,3,4,4aa,9,10,10aa-octahydroanthracene (see Fig. 4, *a*, curves 1, 2). Molecules of each octahydroanthracene isomer can be presented as tetralin-like structures shielded by the cyclohexane "chair" in different manners. Two stereoisomers with the terminal benzene ring are formed in approximately equal amounts (see Fig. 4, *a*, curves 1, 2) but in appreciably smaller amounts than the *sym*-isomer with the central benzene ring. A similar ratio can also be related to a higher reactivity of the terminal rings of octahydroanthracene compared to the central ring. On the one hand, an increase in non-complanarity of the octahydroanthracene isomers stronger impeded hydrogenation but, on the other hand, increases the possible number of hydrogenation routes.

Chromatographic and MS/GC analyses showed that the samples of the reaction products contain five compounds of the general stoichiometric composition  $C_{14}H_{24}$  corresponding to perhydroanthracene conformers (see Fig. 4, *b*, curves 1–5). The overall selectivity to five conformers exceeded 99%, and the complete saturation with hydrogen of the initial anthracene to final perhydroanthracene, under the conditions of certain experiment, was achieved within 38 h after the start of hydrogenation.<sup>22</sup> It is seen from Fig. 3 that the slope of experimental curve III that characterizes the rate of formation of a conventional group of compounds with three saturated rings is smaller than the slope of curves II and I describing the rate of formation of the compounds with two and one saturated rings, respectively.

The obtained experimental data show that the hydrogenation of the studied compounds with fused structures can be presented as a combination of hydrogenation reactions of each benzene ring in naphthalene and anthracene molecules, and optimum conditions differ for each reaction. Based on the time needed to achieve 95% conversion of hydrogenation and ignoring different reaction conditions of hydrogenation of benzene, naphthalene, and anthracene, a series of decreasing activity for these substrates is naphthalene  $\leq$  benzene  $<$  anthracene. The time required to achieve complete hydrogenation increases in the order benzene  $<$  naphthalene  $\ll$  anthracene. A similar decrease in activity correlates with the results obtained earlier for linearly conjugated biphenyl and terphenyl molecules.<sup>2</sup> However, hydrogenation is impeded for fused naphthalene and anthracene molecules because of the enhancement of steric hindrances in the initial molecules and intermediate reaction products, especially at the nodal carbon atoms.

The quantum chemical (DFT) modeling of benzene adsorption on the Pt(111) surface showed that with allowance for the optimization of geometric parameters a stronger interaction ( $E_{\text{ads}} = -0.69$  eV per Pt atom) occurs in the bridge position ( $Bz_2$ ) when the bond is formed with four metal atoms. In  $Bz_1$ , when the benzene molecule forms a bond with three Pt atoms, the adsorption energy

was observed to be  $-0.63$  eV per one Pt atom.<sup>23–25</sup> For naphthalene with two fused benzene rings, the adsorption energy in the dibridge conformation ( $Nph_2$ ) is also higher than that in the conformation  $Nph_1$ :  $-0.67$  and  $-0.5$  eV per one Pt atom, respectively.<sup>23,25</sup>



The adsorption energy of the anthracene molecule in the tribridge configuration ( $Ant_2$ ) was found to be  $-0.71$  eV per one Pt atom.<sup>25</sup> It is seen from comparison that the calculated adsorption energies per one Pt atom for the studied substrates in the bridge conformation increase in the series naphthalene  $\leq$  benzene  $<$  anthracene. Taking into account the total number of Pt atoms necessary for the accomplishment of the corresponding bridge conformations, the order of increasing adsorption energy per molecule is benzene  $<$  naphthalene  $\ll$  anthracene. A comparison of the experimental and theoretical data shows a correlation between the time needed to achieve complete hydrogenation of benzene, naphthalene, and anthracene and calculated adsorption energies of the corresponding molecules on the Pt(111) surface.

To conclude, similar parameters of hydrogenation were obtained on the Pt/C catalysts with different morphologies: on active carbon and carbon support Sibunit. Comparing the experimental data on the hydrogenation of benzene, naphthalene, and anthracene in a direct way and ignoring more stringent reaction conditions, it can be inferred that the times needed to achieve 95% conversion are comparable at the step of hydrogenation of the first benzene ring in planar naphthalene and benzene molecules. Nearly twice as much time was needed to achieve 95% conversion of anthracene as the size of the molecule increased to three rings. As the saturation with hydrogen increases, the cyclohexane ring impart non-complanarity to molecules of the formed intermediates, which favors an increase in steric hindrances and inhibition of the hydrogenation reaction. Under these conditions, nodal C atoms become significant, different hydrogenation conditions of which favor different quantitative ratio of isomers in the final products. In particular, the formation of *cis*- and *trans*-isomers of decalin depends on the orientation of the H atom (to the face or to the side from the surface) in position 10 in the intermediate product octahydronaphthalene (1,9-octalin).<sup>22,26,27</sup> Analyzed samples contained no cracking products in all experiments.

The authors are grateful to the Department of Structure Studies of the N. D. Zelinsky Institute of Organic Chemistry (Russian Academy of Sciences) for investigations of the samples by electron microscopy.

This work was financially supported by the Russian Science Foundation (Project No. 14-50-00126).

## References

1. J. Ren, N. M. Musyoka, H. W. Langmi, M. Mathe, S. Liao, *Int. J. Hydrogen Energy*, 2017, **42**, 289.
2. A. N. Kalenchuk, V. I. Bogdan, S. F. Dunaev, L. M. Kustov, *Fuel Proc. Technol.*, 2018, **169**, 94.
3. A. N. Kalenchuk, V. I. Bogdan, L. M. Kustov, *Russ. J. Phys. Chem. A*, 2015, **89**, 16.
4. A. Stanislaus, B. H. Cooper, *Catal. Rev.-Sci. Eng.*, 1994, **36**, 75.
5. B. H. Cooper, B. B. L. Donnis, *Appl. Catal. A*, 1996, **137**, 203.
6. A. A. Shukla, P. V. Gosavi, J. V. Pande, V. P. Kumar, K. V. R. Chary, R. B. Biniwale, *Int. J. Hydrogen Energy*, 2010, **35**, 4020.
7. M. P. Lazaro, E. G. Bordeje, D. Sebastian, M. J. Lazaro, R. Moliner, *Catal. Today*, 2006, **138**, 203.
8. G. Maria, A. Marin, C. Wyss, S. Muller, E. Newson, *Chem. Eng. Sci.*, 1996, **51**, 2891.
9. A. Bourane, M. Elanany, T. V. Pham, S. P. Katikaneni, *Int. J. Hydrogen Energy*, 2016, **41**, 23075.
10. R. B. Biniwale, S. Rayalua, S. Devotta, M. Ichikawa, *Int. J. Hydrogen Energy*, 2008, **33**, 360.
11. A. A. Balandin, *Multipletnaya teoriay kataliza. Chast' I. Strukturnye factory v katalize* [Multiplet Theory of Catalysis. Part I. Structural Factors in Catalysis], Mos. Gos. Univ., Moscow, 1963, 106 pp. (in Russian).
12. H. I. Waterman, J. J. Leenderste, A. C. Cranendonk, *Recl. Trav. Chim. Pay-Bas.*, 1939, **58**, 83.
13. S. Nishimura, *Handbook of Heterogeneous Catalytic Hydrogenation for Organic Synthesis*, John Wiley & Sons, New York, 2001, 737 pp.
14. J. L. Pinilla, A. B. Garcia, K. Philippot, P. Lara, E. J. Garcia-Suarez, M. Millan, *Fuel*, 2014, **116**, 729.
15. A. N. Kalenchuk, A. E. Koklin, V. I. Bogdan, L. M. Kustov, *Russ. Chem. Bull.*, 2017, **66**, 1208.
16. A. N. Kalenchuk, N. A. Davchan, V. I. Bogdan, S. F. Dunaev, L. M. Kustov, *Russ. Chem. Bull.*, 2018, **67**, 28.
17. A. P. Karnaukhov, *Adsorbtsiya. Tekstura dispersnykh i poristykh materialov* [Adsorption. Texture of Dispersion and Porous Materials], Nauka, Novosibirsk, 1999, 470 pp. (in Russian).
18. A. N. Kalenchuk, V. I. Bogdan, S. F. Dunaev, L. M. Kustov, *Int. J. Hydrogen Energy*, 2018, **43**, 6191.
19. <http://profbeckman.narod.ru/MedMemb.files/medmemb5.pdf>.
20. D. B. Berezin, B. D. Berezin, *Kurs sovremennoi organicheskoi khimii* [The Course of Modern Organic Chemistry], Vysshaya Shkola, Moscow, 1999, 756 pp. (in Russian).
21. S. Toppinen, T. K. Rantakyla, T. Salmi, J. Aittamaa, *Ind. Eng. Chem. Res.*, 1996, **35**, 1824.
22. A. N. Kalenchuk, A. E. Koklin, V. I. Bogdan, V. V. Lunin, *Rus. J. Phys. Chem. A*, 2018, **92**, 663.
23. C. Morin, D. Simon, P. Sautet, *J. Phys. Chem. B*, 2003, **107**, 2995.
24. F. Mittendorfer, C. Thomazeay, P. Raybaud, H. Toulhouat, *J. Phys. Chem. B*, 2003, **107**, 12287.
25. C. Morin, D. Simon, P. Sautet, *J. Phys. Chem. B*, 2004, **108**, 12084.
26. A. W. Weitkamp, *Adv. Catal.*, 1968, **18**, 1.
27. P. Li, Y. L. Huang, D. Chen, J. Zhu, T. J. Zhao, X. G. Zhou, *Catal. Commun.*, 2009, **10**, 815.

Received June 4, 2018;  
accepted June 15, 2018